Filtrated Common Functional Principal Component Analysis of Multigroup Functional Data

JIAO, Shuhao; FROSTIG, Ron; OMBAO, Hernando

Published in:
The Annals of Applied Statistics

Published: 01/06/2024

Document Version:
Final Published version, also known as Publisher's PDF, Publisher's Final version or Version of Record

Published version (DOI):
10.1214/23-AOAS1827

Publication details:
JIAO, S., FROSTIG, R., & OMBAO, H. (2024). Filtrated Common Functional Principal Component Analysis of Multigroup Functional Data. *The Annals of Applied Statistics*, *18*(2), 1160-1177. https://doi.org/10.1214/23-AOAS1827

JIAO, S., FROSTIG, R., & OMBAO, H. (2024). Filtrated Common Functional Principal Component Analysis of Multigroup Functional Data. *The Annals of Applied Statistics, 18*(2), 1160-1177. https://doi.org/10.1214/23-AOAS1827

The Annals of Applied Statistics
2024, Vol. 18, No. 2, 1160–1177
https://doi.org/10.1214/23-AOAS1827

FILTRATED COMMON FUNCTIONAL PRINCIPAL COMPONENT ANALYSIS OF MULTIGROUP FUNCTIONAL DATA

BY SHUHAO JIAO[1,a], RON FROSTIG[2,b] AND HERNANDO OMBAO[3,c]

[1]*Department of Biostatistics, City University of Hong Kong,* [a]*shuhao.jiao@cityu.edu.hk*
[2]*Department of Neurobiology and Behavior, University or California, Irvine,* [b]*rfrostig@uci.edu*
[3]*Statistics Program, King Abdullah University of Science and Technology,* [c]*hernando.ombao@kaust.edu.sa*

Local field potentials (LFPs) are signals that measure electrical activities in localized cortical regions and are collected from multiple tetrodes implanted across a patch on the surface of cortex. Hence, they can be treated as multigroup functional data, where the trajectories collected across temporal epochs from one tetrode are viewed as a group of functions. In many cases multitetrode LFP trajectories contain both global variation patterns (which are shared by most groups, due to signal synchrony) and idiosyncratic variation patterns (common only to a small subset of groups), and such structure is very informative to the data mechanism. Therefore, one goal in this paper is to develop an efficient algorithm that is able to capture and quantify both global and idiosyncratic features. We develop the novel filtrated common functional principal components (filt-fPCA) method, which is a novel forest-structured fPCA for multigroup functional data. A major advantage of the proposed filt-fPCA method is its ability to extract the common components in a flexible "multiresolution" manner. The proposed approach is highly data-driven, and no prior knowledge of "ground-truth" data structure is needed, making it suitable for analyzing complex multigroup functional data. In addition, the filt-fPCA method is able to produce parsimonious, interpretable, and efficient functional reconstruction (low reconstruction error) for multigroup functional data with orthonormal basis functions. Here the proposed filt-fPCA method is employed to study the impact of a shock (induced stroke) on the synchrony structure of rat brain. The proposed filt-fPCA is general and inclusive that can be readily applied to analyze any multigroup functional data, such as multivariate functional data, spatial-temporal data, and longitudinal functional data.

1. Introduction.

1.1. *Data description and statistical challenges*. This work is motivated by a neurobiological experiment conducted by coauthor, Ron Frostig, where the goal is to investigate the impact of an extreme shock (such as a stroke) on the functional organization of rat brain. In the experiment described in Wann (2017), ischemic stroke was simulated by clamping the medial cerebral artery of the rat. Brain activity was continuously monitored over several hours through the local field potential (LFP) recordings from 32 implanted micro-tetrodes (see Figure 1). In this set-up, two temporal phases of the LFP recordings are considered: preocclusion and postocclusion.

One goal in dimension reduction of such functional data is to identify the commonality of covariance structures across different tetrodes, which is highly associated with synchrony in the network of tetrodes in this isolated cortical region. Here we say "covariance structure" instead of "covariance operator" because the major interest is variation pattern rather

Received February 2023; revised September 2023.
Key words and phrases. Functional principal components, community detection, dimension reduction, multigroup functional data, network filtration, weighted network.

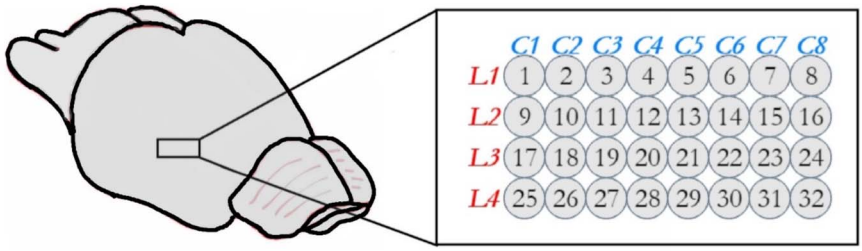

FIG. 1. *Placement of* 32 *tetrodes on the rat cortex.*

than variation magnitude. As the covariance structure of different tetrodes can be similar, due to the synchrony phenomenon, it is possible to employ common principal components across different tetrodes. Such common principal components are informative to the synchrony structure of multitetrode LFPs. Note that signal synchrony is a strong motivation that leads to the feasibility of employing common principal components. Two groups of functions can share common principal components as long as they share similar covariance structure. The new method is developed for general multigroup functional data, not only for synchronized multigroup functions.

In this paper, the focus is on a 10-minute window around the time of occlusion: five minutes immediately prior to occlusion onset of the medial cerebral artery (preocclusion) and five minutes during the postocclusion phase. The aims of our data analysis are: (i.) to extract the commonality structure of variation pattern for both phases respectively and (ii.) to identify and quantify the differences in the commonality structure between the two phases. To conduct our analysis, the LFP data is segmented into one-second epochs, and thus each of the preocclusion and postocclusion phases consists of 300 epochs for each tetrode; see Figure 2 for the diagram of the LFP data.

It is noted that some tetrodes produced trajectories displaying similar variation patterns due to signal synchrony. However, note that the level of synchrony is not the same across all tetrodes. It is critical to examine how the stroke can alter synchrony in the brain. Thus, the hope here is that the proposed filt-fPCA can lead to deeper understanding of how the temporal coordination in the function of large-scale brain networks are associated with the functional impairments caused by ischemia.

1.2. *Existing fPCA methods for multigroup functional data.* Functional data analysis is an active area primarily driven by its wide range of application. Due to the infinite dimensionality of functional data, one of the fundamental techniques employed in the analysis is dimension reduction. Functional principal component analysis (fPCA), as described in Ramsay and Silverman (2005), is a widely-applied dimension reduction technique because it gives the optimal functional reconstruction (with respect to the integrated squared error of reconstruction) and at the same time yields results that are interpretable in the sense that it captures the principal directions of variation. More work on fPCA include Hall and Hosseini-Nasab (2006), Hall, Müller and Wang (2006), Yao and Lee (2006), Yao (2007), Jiang and Wang (2010), Bali et al. (2011).

Several methods of fPCA for multigroup functional data have been recently developed. A multilevel functional principal components method was proposed in Di et al. (2009), which explains the variation both within and between different groups of functions. This was extended to sparse sampled multilevel functional data in Di, Crainiceanu and Jank (2014). In Kayano and Konishi (2009), functional principal component analysis was developed for multivariate functions with Gaussian-shape basis. Berrendero, Justel and Svarc (2011) proposed the multivariate principal component with functional scores. A framework for longitudinal functional principal components in Greven et al. (2010) combines the covariance of

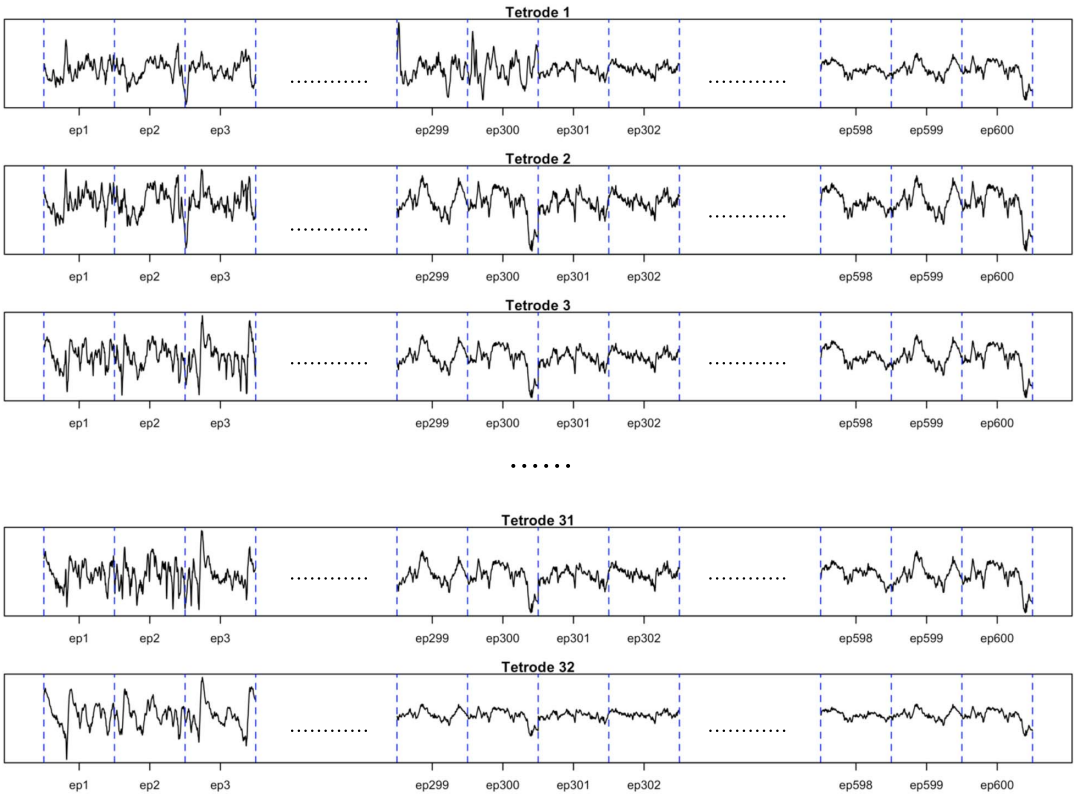

FIG. 2. *Diagram of LFPs. The stroke was induced at the end of the* 300*th epoch* (*ep*300), *each epoch has* 1000 *recordings observed over one second. Synchrony of epochs exists across tetrodes* (*e.g.*, *tetrode* 3, 31, *and* 32).

within-subject and between-subject components. A two-step fPCA method for longitudinal functional data was developed in Chen and Müller (2012), where the fPCA is implemented according to different longitudinal indexes, and the resulting principal components vary as the longitudinal index changes. An extension was proposed in Chen, Delicado and Müller (2017) which gives a framework with a more parsimonious fPC representation—marginal fPC representation. The fPCA in these work is typically developed on some known or presumed data structure. Chiou, Chen and Yang (2014) and Jacques and Preda (2014) proposed the multivariate functional principal component analysis (MfPCA), which describes the variation pattern of multivariate functional data, and Happ and Greven (2018) extended MfPCA for functions defined over different domains. Another track of research, which is more related to our work, is common principal component analysis (CPCA, see, e.g., Flury (1984), Benko, Härdle and Kneip (2009), and Coffey et al. (2011)) and partial common principal component analysis (PCPCA, see, e.g., Flury (1987), Schott (1999), Wang et al. (2021)). The ideas in the following work can also be applied to multigroup functional data. In Crainiceanu et al. (2011), a population value decomposition (PVD) procedure is proposed. Moreover, Lock et al. (2013) and Feng et al. (2018) proposed JIVE and AJIVE procedures to extract common and individual components for multiblock data.

While some of the existing methods (i.e., CPCA and PCPCA) and the proposed filt-fPCA share the same goal of finding a common "representation" of multigroup functional data, the principles and algorithms are different. In CPCA and PCPCA, all groups are assumed to share the same set of common principal components. In practice, this assumption is overly restrictive. Comparatively, filt-fPCA aims to find a "multiresolution" commonality structure, and thus the number of (filtrated) common functional principal components is allowed to vary

across groups. Compared to the existing methods, one advantage of the filt-fPCA method is that it has the ability to produce a more flexible and efficient (low-functional reconstruction error) fPC commonality structure, which identifies global (common across groups) and local (group-specific) features, and works for both balanced and unbalanced designs.

1.3. *Filtrated functional principal component analysis.* In this article we develop a new method to extract common fPCs (filt-fPCs) that produce a low-dimensional representation for multigroup functional data. The filt-fPCA method builds on the idea of filtration in network analysis and extracts the common principal components via multilayer filtrations.

The *fundamental philosophy* of filt-fPCA is that, as the common components are extracted from different groups of functions (in our application the functions are the epoch trajectories, and the epochs collected from the same tetrode are viewed as a group) with an increasing number of layers, the commonality across different groups tends to diminish. Define a *community* as a set of groups that share a common filt-fPC. In the first layer of filtration, all groups are clustered into some (comparatively) big communities. For each of the communities, the common filt-fPC shared by the groups therein are extracted. Then we split these communities into smaller subcommunities (which are, of course, no larger than those in the first layer), and the second common filt-fPCs are extracted. This splitting & extraction procedure is repeated till some ending conditions are satisfied. At the deeper layers of the filtration, "higher-resolution" (more group-specific) common components are going to be extracted. The communities in each layer are always nested in, or identical to, the communities of the previous layer. The filt-fPCs in the first layer of filtration pertain to the most common variation patterns, and the filt-fPCs in the layers formed later pertain to more idiosyncratic variation patterns, which are shared by a fewer number of groups. That is why we adopt forest structure for commonality, as displayed in Figure 3.

Clearly, a primary step before obtaining filt-fPCs is to find reasonable forest-structured communities for commonality structure. Note that the commonality structure, adopted in PCPCA, is a special case of our proposed forest structure. Specifically in PCPCA, in the layers pertaining to commonality, all groups are assigned to the same community, and in the layers pertaining to idiosyncrasy, all groups are separated from each other. In addition, groupwise ordinary fPCs can also be viewed as a special case of filt-fPCs, where all groups are separated from each other in all layers.

In summary, filt-fPCA has the following advantages: (1) The procedure of searching for the optimal forest structure is completely data-driven without constraints of model specification; thus, filt-fPCA is robust to problems with model misspecification, and no prior knowledge is

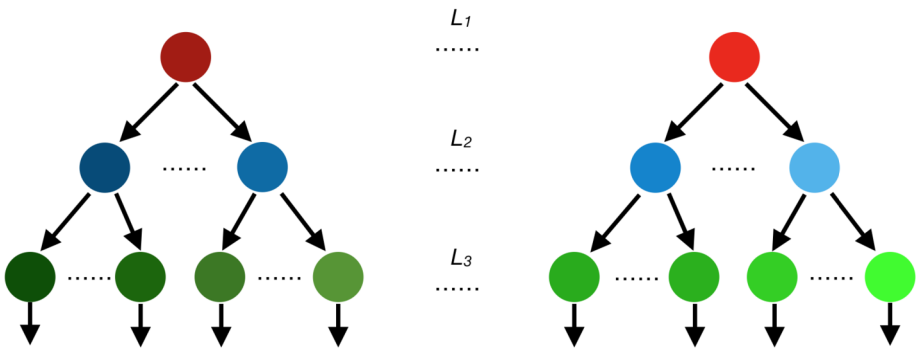

FIG. 3. *Hierarchical forest structure of filt-fPCs. Here L_j signifies the jth layer of filtration. Different communities are represented by different solid circles. Note that there can be multiple trees since the groups may be partitioned into multiple communities in the first layer* (*one tree per first-layer community*).

needed to implement the method. (2) The method simultaneously reveals both common and idiosyncratic features of various groups in a "multiresolution" manner, which enables sophisticated analysis and provides comprehensive explanation of commonality structure. (3) The method produces orthonormal basis functions, which are efficient in functional reconstruction. (4) The proposed method is applicable to both balanced and unbalanced designs.

The rest of the paper is organized as follows. In Section 2 some preliminaries of functional data are introduced. In Section 3 we develop the filt-fPCA algorithm, including network filtration, computation of filt-fPCs, and community detection and selection. Section 4 presents the simulation results. Section 5 presents the real data analysis on the local field potentials of rat brain activity. Conclusions are made in Section 6. Technical proofs, pseudocode, and additional simulation and figures can be found in the Supplementary Material.

2. Preliminaries. Denote $X(t) \in L_H^p = L_H^p(\Omega, \mathcal{A}, \mathbb{P})$ to be such that, for some $p > 0$, a H-valued function $X(t)$ satisfies $E\{\|X(t)\|^p\} < \infty$. Here $\|\cdot\|$ is the ℓ^2-norm defined for elements in H. In what follows, all functions are assumed to be elements in the Hilbert space $L^2[0, 1]$, where the inner product is defined as $\langle x, y\rangle = \int_0^1 x(t)y(t)dt$, and the norm is defined as $\|x\|^2 = \int_0^1 x(t)^2 dt$. Suppose that $X(t) \in L_H^1$, then the mean function is defined to be $\mu(t) = E\{X(t)\}$. Moreover, if $X(t) \in L_H^2$, then the covariance operator is defined to be $\Gamma(\cdot)\colon L^2[0, 1] \to L^2[0, 1]$ by $\Gamma(\cdot) = E\{\langle X - \mu, \cdot\rangle(X - \mu)(t)\}$.

By the Mercer's theorem, $\Gamma(\cdot) = \sum_{j=1}^{\infty} \theta_j \langle \nu_j, \cdot\rangle \nu_j$, where $\{\theta_j\colon j \in \mathbb{N}_+\}$ are the positive eigenvalues (in strictly descending order) and $\{\nu_j(t)\colon j \in \mathbb{N}_+\}$ are the corresponding normalized eigenfunctions, so that $\Gamma(\nu_j) = \theta_j \nu_j$ and $\|\nu_j\| = 1$. Here, $\{\nu_j(t)\colon j \in \mathbb{N}_+\}$ form a sequence of orthonormal bases for $L^2[0, 1]$. Let $\{X_n(t)\colon n \in \mathbb{N}\}$ be a sequence of random functions with mean function $\mu(t)$ and covariance operator $\Gamma(\cdot)$. By the Karhunen-Loève theorem, under mild conditions, $X_n(t)$ admits the representation $X_n(t) = \mu(t) + \sum_{j=1}^{\infty} \langle X_n - \mu, \nu_j\rangle \nu_j(t)$. Suppose that there are N samples $X_1(t), \ldots, X_N(t)$, then the estimator of $\mu(t)$ is $\hat{\mu}(t) = N^{-1} \sum_{n=1}^{N} X_n(t)$, and the estimator of the covariance operator is given by $\widehat{\Gamma}(\cdot) = N^{-1} \sum_{n=1}^{N} \langle X_n - \hat{\mu}, \cdot\rangle(X_n - \hat{\mu})(t)$.

3. Filtrated common functional principal component. In this section we formalize the concept of filt-fPCA and illustrate the implementation details. The section is arranged as follows: (1) the definition and estimation of filt-fPCs (Sections 3.1 and 3.2) and (2) the selection of commonality forest structure (Sections 3.3 and 3.4).

3.1. *The filt-fPC representation.* Suppose that there are G groups of functions $\{X_{vn}(t)\colon n \in \mathbb{N}, v = 1, \ldots, G\}$, where $X_{vn}(t)$ is the nth function in group v. Recall that the primary aim is to obtain the common filt-fPCs shared by groups in each of the communities to be specified, and a community is defined to be a set of groups where one common filt-fPC is employed for all the groups in that set. The key idea of filt-fPCA is to represent $\{X_{vn}(t)\colon v = 1, \ldots, G, n = 1, \ldots, N_v\}$ in the following form:

$$X_{vn}(t) = \mu_v(t) + \sum_{d=1}^{\infty} \langle X_{vn} - \mu_v, \phi_d^{(c_{v,d})}\rangle \phi_d^{(c_{v,d})}(t),$$

where $c_{v,d}$ is the community index of group v in the dth layer of filtration (group v and v' share a common filt-fPC in layer d if $c_{v,d} = c_{v',d}$) and $\{\phi_d^{(c_{v,d})}(t)\colon d \geq 1\}$ specify the directions of filt-fPCs of group v, satisfying $\langle \phi_d^{(c_{v,d})}, \phi_{d'}^{(c_{v,d'})}\rangle = 0$ as $d \neq d'$ and $\|\phi_d^{(c_{v,d})}\| = 1$, and $\mu_v(t)$ is the mean function of the vth group, which is zero in our project since LFPs always oscillate around the zero-line. $\{\langle X_{vn} - \mu_v, \phi_d^{(c_{v,d})}\rangle\colon d \geq 1\}$ are the filt-fPC scores of $X_{vn}(t)$.

REMARK 1. Note that, since functional data is infinite-dimensional, a community structure can include up to infinitely many layers (one layer per dimension). Nevertheless, in practice, only a finite number of layers can be incorporated since it is impractical to conduct statistical analysis in an infinite-dimensional space.

3.2. *Filt-fPCA and estimation*. Without loss of generality, assume the mean function of each group v is zero. Given the forest-structured communities, the estimation of filt-fPCs is easy-to-implement. Denote $\mathcal{K}_{d1}, \mathcal{K}_{d2}, \ldots$ as the communities in the dth layer, and

$$R_{vn}^{(d)}(t) = X_{vn}(t) - \sum_{j=1}^{d} \langle X_{vn}, \phi_j^{(c_{v,j})} \rangle \phi_j^{(c_{v,j})}(t)$$

as the projection residual of $X_{vn}(t)$ in the dth layer, and $\Gamma_v^{(d)}(\cdot)$ as the covariance operator of $R_{vn}^{(d)}(t)$. As a special case, $R_{vn}^{(0)}(t) = X_{vn}(t)$. To achieve efficient functional reconstruction, the direction of the common filt-fPC shared by groups in $\mathcal{K}_{di}$, denoted by $\psi_{di}(t)$, is defined as follows:

$$\psi_{di}(t) = \arg\max_{\|\phi\|=1} \left\langle \sum_{v \in \mathcal{K}_{di}} f_v^{(d-1)} \Gamma_v^{(d-1)}(\phi), \phi \right\rangle,$$

where the quantity to be maximized measures the weighted sum of variation of groups in $\mathcal{K}_{di}$, explained by $\phi(t)$, and the tuning parameters $\{f_v^{(d-1)} : v, d \geq 1\}$ should be prespecified (see Remark 2 for the specification in our application). $\{\phi_d^{(c_{v,d})}(t) : v, d \geq 1\}$ are iteratively estimated as $\hat{\phi}_d^{(c_{v,d})}(t) = \hat{\psi}_{di}(t)$ if $v \in \mathcal{K}_{di}$ in layer d, where

$$\hat{\psi}_{di}(t) = \arg\max_{\|\phi\|=1} \sum_{v \in \mathcal{K}_{di}} \sum_{n=1}^{N_v} \frac{f_v^{(d-1)}}{N_v} \langle \widehat{R}_{vn}^{(d-1)}, \phi \rangle^2 \quad \text{for } v \in \mathcal{K}_{di}, i \geq 1,$$

and

$$\widehat{R}_{vn}^{(d-1)}(t) = \begin{cases} X_{vn}(t) - \sum_{j=1}^{d-1} \langle X_{vn}, \hat{\phi}_j^{(c_{v,j})} \rangle \hat{\phi}_j^{(c_{v,j})}(t) & \text{if } d \geq 2, \\ X_{vn}(t) & \text{if } d = 1. \end{cases}$$

The maximizer of the objective $\sum_{v \in \mathcal{K}_{di}} \sum_{n=1}^{N_v} N_v^{-1} f_v^{(d-1)} \langle \widehat{R}_{vn}^{(d-1)}, \phi \rangle^2$ is the first eigenfunction of the operator $\sum_{v \in \mathcal{K}_{di}} f_v^{(d-1)} \widehat{\Gamma}_v^{(d-1)}(\cdot)$, where

$$\widehat{\Gamma}_v^{(d-1)}(\cdot) = N_v^{-1} \sum_{n=1}^{N_v} \{ \widehat{R}_{vn}^{(d-1)} \langle \widehat{R}_{vn}^{(d-1)}, \cdot \rangle \}.$$

Then, given $\{\hat{\phi}_d^{(c_{v,d})} : d \geq 1\}$ and total number of layers D, the reconstruction of $X_{vn}(t)$ is given by

$$X_{vn}(t) \approx \mu_v(t) + \sum_{d=1}^{D} \langle X_{vn} - \mu_v, \hat{\phi}_d^{(c_{v,d})} \rangle \hat{\phi}_d^{(c_{v,d})}(t).$$

The selection of D and community structure will be discussed in Section 3.4.

REMARK 2. $\{f_v^{(d-1)} : v, d \geq 1\}$ should be specified a priori, and they indicate the importance of different groups in different layers. In our application $f_v^{(0)} = 1/\sum_{j \geq 1} \theta_{vj}^{(0)}$, where

$\theta_{vj}^{(d)}$ is the jth eigenvalue of the covariance operator of $R_{vn}^{(d)}$. We scale all groups in the first layer so that the groups with higher variation do not lay higher influence on the common filt-fPCs. For the other layers, $f_v^{(d)} = 1$. The reason is that if group v was not well explained in layer d, the variation of residuals $\{R_{vn}^{(d)} : n \geq 1\}$ would be higher, and then group v would lay higher influence on the common filt-fPC in layer $d+1$, making it more likely to be well explained in layer $d+1$.

PROPOSITION 3.1. *$\{\hat{\phi}_d^{(c_{v,d})}(t) : d \geq 1\}$ are orthonormal for any $v \geq 1$.*

This proposition is important in sequential analysis, for example, in the finite-dimensional representation of functional linear models, orthonormality avoids cross terms and hence leads to a concise finite-dimensional representation.

3.3. *Weighted network, filtration, and community detection.* As discussed in Section 3.2, one advantage of the filt-fPCA is that it is easy-to-implement once the community structure is obtained. The procedure of obtaining the community structure is decomposed into three main steps: (1) establish a weighted network to evaluate the similarity of covariance structure, (2) filtrate the weighted network to obtain a sequence of subnetworks, and (3) apply community detection to each subnetwork to obtain the community structure in the associated layer. The three steps are discussed in details below.

The preliminary step of network establishment is to evaluate the similarity of covariance structure of different groups. A weighted network is a triple $(N, E, \boldsymbol{\omega})$, where N is the node set representing groups, E is the edge set, and $\boldsymbol{\omega}$ is the set of edge weights. In our application one node represents one group; edges can be viewed as existence of synchrony between different regions of brain, which is complete (all pairs of nodes are connected) at the beginning of filtration since we have no prior knowledge on which tetrodes are not synchronized at all; weights represent the similarity of covariance structures and also reveal the scale of synchrony. A *small* value of edge weight indicates *high* level of synchrony between the adjacent nodes. In principle, if two nodes are connected by an edge, then the functions in the two associated groups share some common filt-fPCs more likely. The edge weight ω should be a reasonable measure of similarity of variation pattern. Notationally, denote the weight of edge adjacent to nodes i and j as ω_{ij}, and we propose to set $\omega_{ij} = \|\mathcal{C}_i - \mathcal{C}_j\|_{\mathcal{S}}$, where $\mathcal{C}_i$ is the scaled covariance operator of the ith group $\mathcal{C}_i = \Gamma_i^{(0)} / \sum_{j\geq 1} \theta_{ij}^{(0)}$, where $\theta_{ij}^{(0)}$ is the jth eigenvalue of $\Gamma_i^{(0)}$, and $\|\cdot\|_{\mathcal{S}}$ denotes the Hilbert–Schmidt norm.

Network filtration is a multithresholding framework for displaying the dynamic pattern of how network features change over different thresholds. Here we specify a sequence of positive thresholds $\{\tau_d : d \geq 1\}$ in nonascending order $(\tau_1 \geq \tau_2 \geq \tau_3 \geq \cdots)$, and one threshold pertains to one layer. For each layer d, we eliminate the edges of which the weights are greater than the threshold τ_d. Corresponding to the thresholds, a sequence of nested subnetworks are obtained after the edge truncation $\{(N, E_d, \boldsymbol{\omega}) : d \geq 1\}$, where $E_1 \supseteq E_2 \supseteq \ldots$.

The last step is to apply some community detection algorithm to separate the nodes into disjoint communities for each $(N, E_d, \boldsymbol{\omega})$. The community detection algorithm applicable here is not unique. We introduce our method in the Supplementary Material (Jiao, Frostig and Ombao (2024)). Since the focus of this paper is not to develop a new community detection algorithm, we do not introduce more details. We illustrate the procedure in an example in Figure 4.

REMARK 3. Before searching the communities in the next layer, a large weight (e.g., $G \times \max_{i,j} \omega_{ij}$) can be set to the edges connecting different communities in the current layer, so that the selected communities in the next layer are always nested in the communities of the current layer.

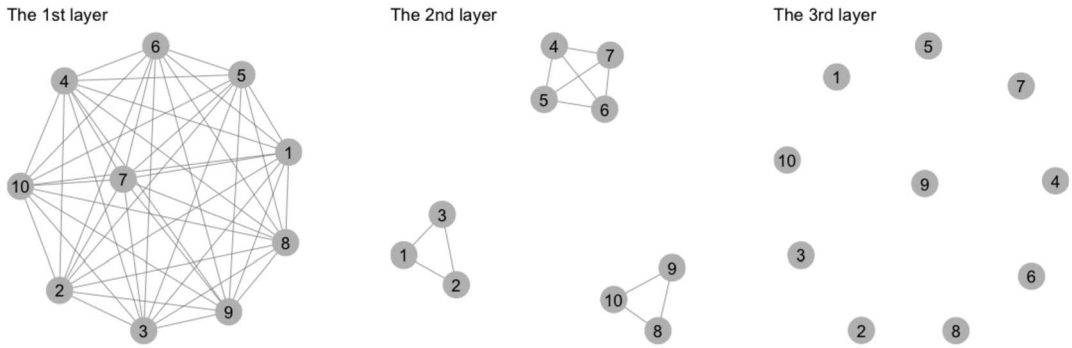

FIG. 4. *Network filtration and the community structure of the first three layers* (10 *groups*). *In the first and second filtration layer, the nodes are separated into one and three communities, and thus one and three common filt-fPCs are obtained in the first two layers respectively. The third layer's filtration eliminates all the edges, and the filt-fPCs, starting from the third layer, pertain to the idiosyncratic variation pattern of each individual group.*

3.4. *Selection of community structure.*

3.4.1. *Generalized information criterion.* Motivated by the generalized information criterion (GIC, see, e.g., Nishii (1984) and Zhang, Li and Tsai (2010)), we propose a penalized criterion, which follows the format:

$$\text{measure of model fit} + \text{tuning parameter} \times \text{measure of model complexity}.$$

The idea behind this penalized criterion is that, if the groups were split into too many communities, the resulting filt-fPCs would very likely fail to capture the commonality of covariance structures, although they are efficient in functional reconstruction.

For a given community structure $\boldsymbol{C}_\alpha$ (α is the index of community structure) and the corresponding $\{\hat{\phi}_{\alpha,d}^{(c_{v,d})}(t), d \geq 1, v = 1, \ldots, G\}$, we define the GIC value to be

$$\text{GIC}(\boldsymbol{C}_{\alpha,1:D}) = -\sum_{v=1}^{G} N_v^{-1} \left\{ \sum_{n=1}^{N_v} \sum_{d=1}^{D} \langle X_{vn}, \hat{\phi}_{\alpha,d}^{(c_{v,d})} \rangle^2 \right\} + \lambda_N(\aleph \boldsymbol{C}_{\alpha,1:D}), \tag{1}$$

where $\aleph$ signifies the cardinality (the total number of communities) and $\boldsymbol{C}_{\alpha,1:D}$ represents the first D layers of community structure $\boldsymbol{C}_\alpha$. Given D, the community structure to be selected should minimize $\text{GIC}(\boldsymbol{C}_{\alpha,1:D})$.

To illustrate the asymptotic properties of the selected community structure, we now introduce the following concept. Let $\{\phi_{vd} : d \geq 1\}$ be the directions of groupwise ordinary fPCs of the vth group, and the following concept quantifies the difference between the filt-fPCs and groupwise ordinary fPCs.

DEFINITION 3.1 (τ-oracle community structure). A community structure $\widetilde{\boldsymbol{C}}_\tau$ is termed a τ-oracle community structure if

$$\sigma_{\alpha,D} := E\left\{ \sum_{v=1}^{G} \sum_{d=1}^{D} \left(\langle X_{vn}, \phi_{vd} \rangle^2 - \langle X_{vn}, \phi_{\alpha,d}^{(c_{v,d})} \rangle^2 \right) \right\} = O(D^{-\tau}).$$

A τ-oracle community structure may not be unique; however, this should not be viewed as a problem, because the main goal here is to find a reasonable community structure but not to find an unknown prespecified community structure.

Given a value of τ specified by the oracle, community structures are classified into three categories—$\mathcal{H}_{\tau,-}$ (under-fitted), $\mathcal{H}_\tau$ (τ-oracle) and $\mathcal{H}_{\tau,+}$ (over-fitted)—defined, respectively, as

$$\begin{aligned}\mathcal{H}_{\tau,-} &= \{\boldsymbol{C}_\alpha : \sigma_{\alpha,D} = O(D^{-\beta_{1,\alpha}}), \beta_{1,\alpha} < \tau\},\\ \mathcal{H}_\tau &= \{\boldsymbol{C}_\alpha : \sigma_{\alpha,D} = O(D^{-\tau})\},\\ \mathcal{H}_{\tau,+} &= \{\boldsymbol{C}_\alpha : \sigma_{\alpha,D} = O(D^{-\beta_{2,\alpha}}), \beta_{2,\alpha} > \tau\},\end{aligned}$$

and define $M = G^{-1}\sum_{v=1}^{G} N_v$,

$$\begin{aligned}\underline{\Delta}\aleph_{\alpha,D}^{\tau} &= \min_{\widetilde{\boldsymbol{C}}_\tau \in \mathcal{H}_\tau} \{\aleph \boldsymbol{C}_{\alpha,1:D} - \aleph \widetilde{\boldsymbol{C}}_{\tau,1:D}\},\\ \overline{\Delta}\aleph_{\alpha,D}^{\tau} &= \max_{\widetilde{\boldsymbol{C}}_\tau \in \mathcal{H}_\tau} \{\aleph \boldsymbol{C}_{\alpha,1:D} - \aleph \widetilde{\boldsymbol{C}}_{\tau,1:D}\}.\end{aligned}$$

With Assumptions (1)–(6) (see the Supplementary Material, Jiao, Frostig and Ombao (2024)), we develop the theorem below, which essentially demonstrates how the selection of the tuning parameter λ_N influences the efficiency of functional reconstruction of the resulting filt-fPCs. The proofs are in the Supplementary Material.

THEOREM 3.2. *Suppose that Assumptions* (1)–(6) *hold, and* $\mathcal{H}_\tau \neq \varnothing$, *if* λ_N *satisfies the following conditions*:

$$\begin{aligned}\max_\alpha \{M^{\beta_{1,\alpha}/\gamma}\overline{\Delta}\aleph_{\alpha,D}^{\tau}\}\lambda_N \to 0, \quad \boldsymbol{C}_\alpha \in \mathcal{H}_{\tau,-},\\ M^{\tau/\gamma}\min_\alpha \{\underline{\Delta}\aleph_{\alpha,D}^{\tau}\}\lambda_N \to \infty, \quad \boldsymbol{C}_\alpha \in \mathcal{H}_{\tau,+},\end{aligned}$$

the selected community structure is a τ*-oracle community structure asymptotically almost surely.*

A drawback of the selection procedure based on the above GIC criterion is that there are a lot of possible community structures when G and D are large, making it very computationally costly to obtain the GIC values for all structures. To overcome this limitation, we propose another iterative procedure described below.

3.4.2. *Iterative selection of thresholds*. In the algorithm each threshold determines the community structure of one layer. Thus, we propose the following iterative selection procedure. Denote the empirical filt-fPC score of $X_{vn}(t)$ in layer d as $Z_{vn,d} = \langle R_{vn}^{(d-1)}, \hat{\phi}_d^{(c_{v,d})}\rangle$, and the GIC value at layer d is

$$\mathrm{GIC}(\boldsymbol{C}_{\alpha,d}) = -\sum_{v=1}^{G}\left\{N_v^{-1}\sum_{n=1}^{N_v} Z_{vn,d}^2\right\} + \kappa_N(d)\aleph \boldsymbol{C}_{\alpha,d}.$$

Here $\kappa_N(d)$ is a nonincreasing function with respect to d; thus, more idiosyncratic features are to be extracted as d increases. We propose to select the threshold τ_d such that the resulting $\widehat{\boldsymbol{C}}_{\alpha,d}$ and $\{\hat{\phi}_d^{(c_{v,d})}(t) : v = 1, \ldots, G\}$ minimize the above quantity. Suppose that the $(d-1)$th threshold is τ_{d-1}, then the dth threshold is searched along the interval $[0, \tau_{d-1}]$. Note that a common threshold can be employed for consecutive multiple, or even infinitely many, layers. In order to minimize computational burden, the thresholds are selected from a finite number of threshold candidates, where each candidate truncates at least one more edge than the larger ones.

Denote the community structure selected by the iterative procedure as $\widehat{\boldsymbol{C}}_{\text{iter}}$. The following theorem demonstrates that, under some regularity conditions on $\{\kappa_N(d)\colon d \geq 1\}$, the iteratively selected community structure will not fall into the underfitted class if the sample size is large enough, which theoretically guarantees efficient functional reconstruction of filt-fPCs selected by the iterative procedure.

THEOREM 3.3. *If Assumptions* (1)—(6) *hold and* $\lambda_N = \sum_{d\geq 1}\kappa_N(d)$ *satisfies the first condition in Theorem* 3.2, *say*, $\max_\alpha\{M^{\beta_{1,\alpha}/\gamma}\overline{\Delta}\aleph^{\tau}_{\alpha,D}\}\lambda_N \to 0$, *for* $\boldsymbol{C}_\alpha \in \mathcal{H}_{\tau,-}$. *Additionally, if* $M^{-1/2}\sum_{d=1}^{D} d^p\kappa_N^{-1}(d) \to 0$, *then* $\widehat{\boldsymbol{C}}_{\text{iter}} \notin \mathcal{H}_{\tau,-}$ *asymptotically almost surely.*

3.4.3. *Selection of D and* $\kappa_N(d)$. In principle, the dimension D is selected so that the first D filt-fPCs capture the most variation for each group. Since ordinary groupwise fPCs are optimal in functional reconstruction, we propose to use the reconstruction by ordinary fPCs as the baseline and make the reconstruction by filt-fPCs close to it. Thus, D is selected so that the first D ordinary fPCs explain a sufficient proportion of variation (e.g., $\sum_{j=1}^{D}\hat{\theta}_{vj}^{(0)}/\sum_{j\geq 1}\hat{\theta}_{vj}^{(0)} > 90\%$) for each group v.

The values of $\{\kappa_N(d)\colon d \geq 1\}$ should be selected so that the resulting community structure is parsimonious (small cardinality) and, meanwhile, leads to efficient filt-fPC reconstruction. Therefore, we first specify some candidates of $\{\kappa_N(d)\colon d \geq 1\}$ and then find those leading to filt-fPCs that explain a sufficient proportion (e.g., 90%) of variation explained by the ordinary groupwise fPCs. Then among the candidates satisfying this condition, we select the ones associated with the community structure which has the smallest cardinality.

It is noted that the number of tuning parameters $\{\kappa_N(d)\colon d = 1, \ldots, D\}$ increases with D. To reduce the complexity of tuning parameter selection, we propose to employ some parametric form for $\kappa_N(d)$, for example, $\kappa_N(d) = ad^{-b}$ and $\kappa_N(d) = a/(1 + b^{d-u})$. A large-valued and slow-decaying sequence $\{\kappa_N(d)\colon d \geq 1\}$ typically leads to a parsimonious but inefficient filt-fPC representation. The advantage of employing parametric form is that we only need to specify candidates for only a few tuning parameters (e.g., a, b, u), then all $\kappa_N(d)$'s will be specified.

4. Simulation studies. The goal here is to investigate the ability of filt-fPCs to capture underlying commonality structure of multigroup functions. In the simulation samples are generated from the following model $X_{vn}(t) = \sum_{d=1}^{5}\xi_{vn,d}h_{vd}(t)$. Five hundred functions are simulated for each of the 16 groups $(\Pi_1, \ldots, \Pi_{16})$. The basis functions $\{h_{vd}(t)\colon v \geq 1, d \geq 1\}$ are selected from 22 simulated orthonormal functions $\{B_1(t), \ldots, B_{22}(t)\}$. The scores $\{\xi_{vn,d}\colon d = 1, \ldots, 5\}$ are independent and follow normal distribution $\mathcal{N}(0, 1.2^{-d})$ for $v = 1, \ldots, 12$, and $\mathcal{N}(0, 1.2^{d-6})$, for $v = 13, \ldots, 16$. The five basis functions employed to generate functions in each group are shown in Table 1. The two halves are identical, but groups 13–16 do not share the same covariance functions of groups 5–8, as the scores follow different distributions. Typically, two groups v, v' have similar covariance structure if they have: (1) similar basis functions $\{h_{vd}(t)\colon d = 1, \ldots, 5\}$ and (2) similar covariance structure of scores $\{\xi_{vn,d}\colon d = 1, \ldots, 5\}$.

The iterative GIC criterion is employed to detect the community structure and the penalty term $\kappa(d) = ad^{-b}$. The selected candidates for a are 0.05, 0.1, 0.2, 0.3, 0.5, and for b are 1, 1.1, 1.2, 1.3, 1.4. Here we use the ratio

$$R = \sum_{v=1}^{16}\sum_{n=1}^{500}\|R_{vn}^{(5)}\|^2 \Big/ \sum_{v=1}^{16}\sum_{n=1}^{500}\|X_{vn}\|^2$$

TABLE 1
Basis functions of different groups

v	$\{h_{vd}(t): d=1,2,3,4,5\}$					v	$\{h_{vd}(t): d=1,2,3,4,5\}$				
1	$B_1(t)$	$B_2(t)$	$B_3(t)$	$B_4(t)$	$B_5(t)$	9	$B_1(t)$	$B_2(t)$	$B_3(t)$	$B_4(t)$	$B_5(t)$
2	$B_1(t)$	$B_2(t)$	$B_3(t)$	$B_4(t)$	$B_6(t)$	10	$B_1(t)$	$B_2(t)$	$B_3(t)$	$B_4(t)$	$B_6(t)$
3	$B_1(t)$	$B_2(t)$	$B_7(t)$	$B_8(t)$	$B_9(t)$	11	$B_1(t)$	$B_2(t)$	$B_7(t)$	$B_8(t)$	$B_9(t)$
4	$B_1(t)$	$B_2(t)$	$B_7(t)$	$B_8(t)$	$B_{10}(t)$	12	$B_1(t)$	$B_2(t)$	$B_7(t)$	$B_8(t)$	$B_{10}(t)$
5	$B_1(t)$	$B_{11}(t)$	$B_{12}(t)$	$B_{13}(t)$	$B_{14}(t)$	13	$B_1(t)$	$B_{11}(t)$	$B_{12}(t)$	$B_{13}(t)$	$B_{14}(t)$
6	$B_1(t)$	$B_{11}(t)$	$B_{12}(t)$	$B_{15}(t)$	$B_{16}(t)$	14	$B_1(t)$	$B_{11}(t)$	$B_{12}(t)$	$B_{15}(t)$	$B_{16}(t)$
7	$B_1(t)$	$B_{11}(t)$	$B_{17}(t)$	$B_{18}(t)$	$B_{19}(t)$	15	$B_1(t)$	$B_{11}(t)$	$B_{17}(t)$	$B_{18}(t)$	$B_{19}(t)$
8	$B_1(t)$	$B_{11}(t)$	$B_{20}(t)$	$B_{21}(t)$	$B_{22}(t)$	16	$B_1(t)$	$B_{11}(t)$	$B_{20}(t)$	$B_{21}(t)$	$B_{22}(t)$

to evaluate the reconstruction performance. The corresponding ratio R, associated with different pairs of a, b, are displayed in Table 2. The result is robust to the selection of the tuning parameters a, b.

Note that the reconstruction accuracy is improved as the penalty values decrease. This is because smaller values of penalty lead to more communities, which makes filt-fPCs more idiosyncratic and increases the reconstruction efficiency at the cost of reduced ability to explain commonality. A reasonable selection of a, b is 0.1, 1.2, since the reconstruction accuracy cannot be substantially improved by incorporating more communities. The selected community structure is displayed below:

$$
\begin{aligned}
\text{First layer}: &\ (\Pi_1\text{–}\Pi_{16}),\\
\text{Second layer}: &\ (\Pi_1\text{–}\Pi_4, \Pi_9\text{–}\Pi_{12});\ (\Pi_5\text{–}\Pi_8, \Pi_{13}\text{–}\Pi_{16}),\\
\text{Third layer}: &\ (\Pi_1, \Pi_2, \Pi_9, \Pi_{10});\ (\Pi_3, \Pi_4, \Pi_{11}, \Pi_{12});\\
&\ (\Pi_5, \Pi_{13});\ (\Pi_6, \Pi_{14});\ (\Pi_7, \Pi_{15});\ (\Pi_8, \Pi_{16}),\\
\text{Fourth layer}: &\ (\Pi_1, \Pi_2, \Pi_9, \Pi_{10});\ (\Pi_3, \Pi_4, \Pi_{11}, \Pi_{12});\\
&\ (\Pi_5, \Pi_{13});\ (\Pi_6, \Pi_{14});\ (\Pi_7, \Pi_{15});\ (\Pi_8, \Pi_{16}),\\
\text{Fifth layer}: &\ (\Pi_1, \Pi_9);\ (\Pi_2, \Pi_{10});\ (\Pi_3, \Pi_{11});\ (\Pi_4, \Pi_{12});\\
&\ (\Pi_5);\ (\Pi_6);\ (\Pi_7);\ (\Pi_8);\ (\Pi_{13});\ (\Pi_{14});\ (\Pi_{15});\ (\Pi_{16}).
\end{aligned}
$$

The first layer extracts the most common components driven by $B_1(t)$. Since $B_1(t)$ is shared by all groups, there is only one community in the first layer. The second common components are driven by $B_2(t)$ and $B_{11}(t)$, so there are two communities in the second

TABLE 2
R values (%) associated with each pair of a, b, the values in the parentheses are the associated cardinality of community structure

	b				
a	1	1.1	1.2	1.3	1.4
0.05	0.041 (35)	0.041 (35)	0.040 (42)	0.040 (42)	0.040 (42)
0.1	3.291 (21)	0.037 (27)	0.037 (27)	0.041 (33)	0.041 (33)
0.2	3.291 (21)	3.291 (21)	3.291 (21)	3.291 (21)	0.037 (27)
0.3	5.089 (19)	3.291 (21)	3.291 (21)	3.291 (21)	3.291 (21)
0.5	18.27 (13)	9.470 (17)	9.470 (17)	5.089 (19)	5.089 (19)

layer. Similar to other layers, the community structure depends on the commonality of basis functions. The selected forest structure provides a decent description of the simulated commonality structure.

The total variation is sufficiently explained with a total of five layers since the functions are simulated with five orthonormal bases. The estimated filt-fPCs and the simulated basis functions, the average norm of reconstruction residuals $r_{vn}^{(d)}(t) = X_{vn}(t) - \sum_{j=1}^{d} \langle X_{nv}, \phi_j^{(c_{v,j})} \rangle \phi_j^{(c_{v,j})}$, and the boxplots of the filt-fPC scores are given in the Supplementary Material. Figure 1 (Supplementary Material) shows that the obtained filt-fPCs are able to explain nearly 100% variation for each group. Figure 2 (Supplementary Material) displays the variance of the filt-fPC scores. In Figure 3 (Supplementary Material), it is clear that the directions of the estimated filt-fPCs are similar to the simulated basis functions, which also justifies the efficiency of filt-fPCs in functional reconstruction.

The partial common functional principal component analysis (PCfPCA) is implemented for comparison and is estimated with the semiparametric method proposed by Wang et al. (2021). The number of common fPCs (denoted by #CPC) takes value in $1, 2, \ldots, 5$ (the PCfPC model degenerates to a CfPC model when there are five common fPCs). Specifically, in PCfPCA we assume that

$$X_{vn}(t) = \begin{cases} \displaystyle\sum_{d=1}^{\#\mathrm{CPC}} \xi_{vn,d}\phi_d + \sum_{d=\#\mathrm{CPC}+1}^{5} \xi_{vn,d}\phi_{vd} & \text{if } \#\mathrm{CPC} < 5, \\ \displaystyle\sum_{d=1}^{5} \xi_{vn,d}\phi_d & \text{if } \#\mathrm{CPC} = 5, \end{cases}$$

where $\langle \phi_d, \phi_{d'} \rangle = 0$ for $d \neq d'$, $\langle \phi_d, \phi_{vd'} \rangle = 0$ for $d' > d$, and ϕ_d, $\phi_{vd'}$ are normalized functions.

The corresponding R values are shown in Table 3. Note that, only when there is one common fPC, the reconstruction accuracy is decent. This is because there is only one common basis function across all the groups, and other common basis functions are shared by only partial groups. Clearly, PCfPCA is not sufficient to explain such complex commonality structure.

In CfPCA/PCfPCA, all groups share the same set of common fPCs. However, such simple model is not sufficient to explain complex commonality structure. The proposed filt-fPCA offers a solution to this problem by providing a multiresolution commonality structure to solve the limitation of CfPCA/PCfPCA. For fair comparison we check the performance of filt-fPCA in another setting where PCfPCA works perfectly, and the results are reported in the Supplementary Material.

REMARK 4. In the simulation functions are generated by a prespecified model. However, in practice, such "ground-truth" generative models are usually unknown. The goal of filt-fPCA is not to find the "ground-truth," since it is very hard to find it among all possible commonality structures. Rather, the goal here is to develop an efficient algorithm to find a reasonable and effective commonality structure to interpret data mechanism.

TABLE 3
R values (%) of PCfPC model with different number of common fPCs, and the values in the parentheses are the associated cardinality of community structure

#CPC	1	2	3	4	5
R	0.006 (65)	7.417 (50)	14.62 (35)	28.94 (20)	45.01 (5)

5. The analysis of rat brain local field potentials.

5.1. *Data processing and visualization.* Synchrony in brain signals exist across brain networks and is an important measure of brain coordination. A suddenly increased scale of synchrony can indicate a rapidly emerging response to an extreme shock such as stroke. Here filt-fPCA is applied to analyze the changes in the synchrony structure of LFP trajectories.

The LFPs were first bandpass-filtered at (0, 50] Hertz and then segmented into one-second epochs. The same procedure can also be employed to other frequency bands, but we did not pursue it here. In the situation where structural breaks in the covariance structure are also of major concern, the first step is to detect these breakpoints (e.g., Jiao, Frostig and Ombao (2023)) and then to apply the method to each local quasi-stationary subsequence segmented by the detected break points. Here the major interest is on the overall difference of variation pattern and hidden community structure between the preocclusion and postocclusion epochs, so we conducted a global analysis for each phase.

A total of 25 layers were considered since the first 25 groupwise ordinary fPCs explain over 90% data variation for each group. Outlier epochs were removed from each tetrode for both phases, where outlier epochs in each group are defined as those of which the l^2-norm is beyond the interval $[Q_1 - 1.5 \times \mathrm{IQR}, Q_3 + 1.5 \times \mathrm{IQR}]$. Here $\mathrm{IQR} = Q_3 - Q_1$ and Q_1, Q_3 are the first and third quantile of the l_2-norm of the epoch trajectories.

Figure 5 displays the edge weights $\omega_{ij}^{(k)} = \|\mathcal{C}_i^{(k)} - \mathcal{C}_j^{(k)}\|_{\mathcal{S}}$, $k = 1, 2$, $i, j = 1, \ldots, 32$. Here $k = 1$ refers to the preocclusion phase, and $k = 2$ refers to the postocclusion phase. Figure 6 shows the average weights defined as $\sum_{j=1}^{32} \omega_{ij}^{(k)}/32$, $i = 1, 2, \ldots, 32$. After the occlusion onset, we see that the epoch trajectories from most of the 32 tetrodes display more similar variation patterns due to the increased scale of synchrony. Therefore, a more parsimonious filt-fPC representation is expected for the postocclusion phase. The weight matrix changes substantially after the occlusion onset, making it necessary to implement filt-fPCA to the two phases separately. We justified the necessity of comparison through a permutation test on the change in weight matrix, and the details can be found in the Supplementary Material.

5.2. *Community structure and filt-fPCs.* The iterative GIC selection procedure was employed to select the community structure. To conduct a fair comparison, the same set of tuning parameters were employed for both phases. Figures 7 and 8 show the communities (first eight layers) of the two phases, where the points (representing tetrodes, displayed in the same order as in the experiment) with the same color and shape are in the same community. Clearly,

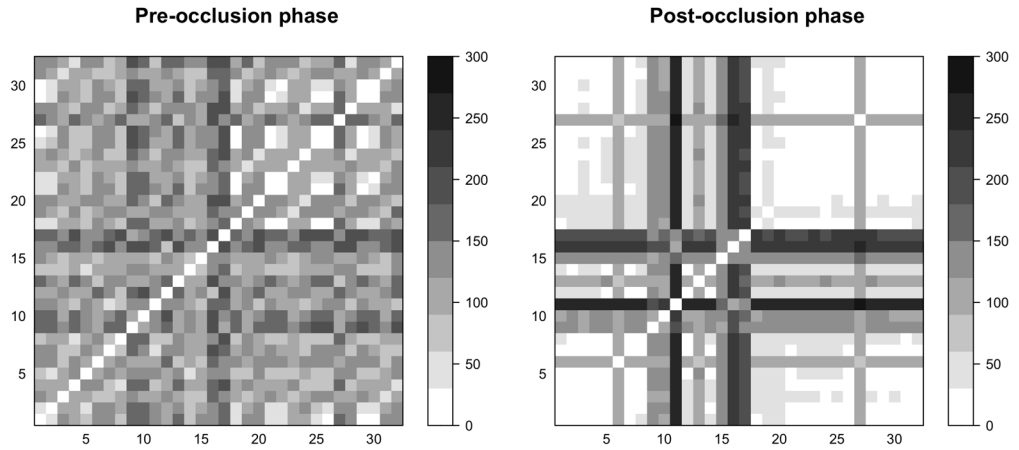

FIG. 5. *Network weights for the two phases.*

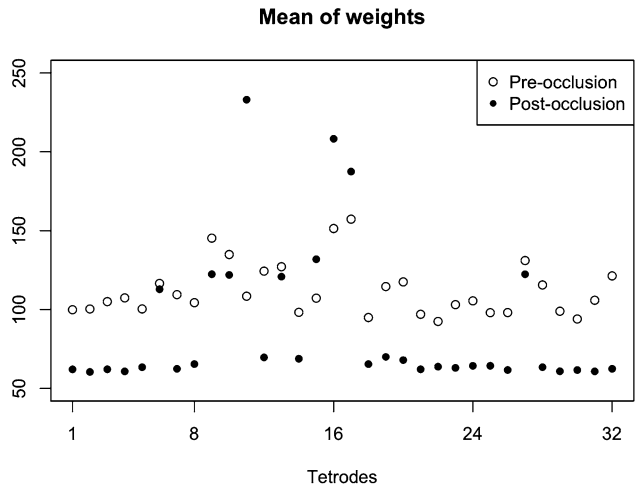

FIG. 6. *Average weights of edges adjacent to each node.*

after the occlusion onset, more tetrodes are clustered in the same community, and the cardinality of community structure drops from 331 to 202 after the occlusion onset (25 layers). One interpretation is that the sudden lack of oxygen delivered caused the neurons to respond in a similar manner. It is interesting that this phenomenon is also observed in financial data; that is, a severe drop in the market elicits similar and synchronized behavior in stocks. The directions of the first five layers' filt-fPCs are presented in Figure 9. It is noted that the first few filt-fPCs explain low-frequency oscillations, and this coincides with the preknowledge that the synchrony is mainly driven by low frequencies (see Wann (2017)).

Before the occlusion onset, the tetrode (1, 2, 18, 21, 22, 25, 26, 29, 30), (24, 28, 32), (3, 31), (4, 8), (7, 11), and (19, 23) are consistently clustered in the same community, respectively, across the 25 layers, and after the occlusion onset, the tetrode (1–5, 7, 8, 12, 14, 29), (18–26, 28, 30–32) are consistently clustered in the same community, respectively. The brain subregions across the tetrodes in the same community are potentially strongly interconnected.

5.3. *Reconstruction efficiency of filt-fPCs.* To show the efficiency of the obtained filt-fPCs in functional reconstruction, we checked the difference between the reconstruction by the filt-fPCs and that by the partial common fPCs. Specifically, we compute the following

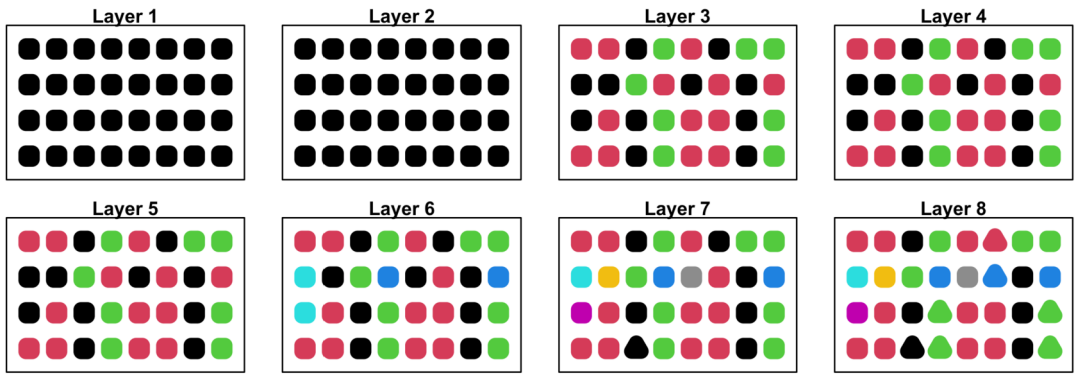

FIG. 7. *Community structures of preocclusion phase (the first eight layers).*

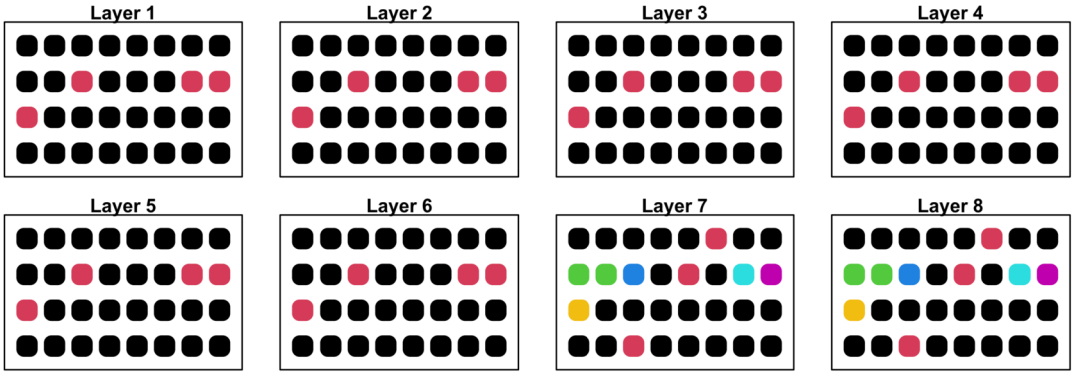

FIG. 8. *Community structures of postocclusion phase (the first eight layers).*

values for different v and D to evaluate reconstruction efficiency:

$$e_{v,D}^{(k)} = \frac{\|\frac{1}{N_v}\sum_{n=1}^{N_v}\sum_{d=1}^{D}\langle X_{vn}^{(k)}, \hat{\phi}_{vd}\rangle\|^2 - \|\frac{1}{N_v}\sum_{n=1}^{N_v}\sum_{d=1}^{D}\langle X_{vn}^{(k)}, \hat{\phi}_{d}^{(c_{v,d})}\rangle\|^2}{\|\frac{1}{N_v}\sum_{n=1}^{N_v}\sum_{d=1}^{25}\langle X_{vn}^{(k)}, \hat{\phi}_{vd}\rangle\|^2},$$

where $\hat{\phi}_d^{(c_{v,d})}$ denotes the direction of filt-fPC or PCfPC. By the method in Wang et al. (2021), there are 12 and 22 common fPCs detected for the preocclusion and postocclusion phase, respectively. Since groupwise ordinary fPCs are optimal in functional reconstruction, they serve as the baseline of comparison, and a small value of $e_{v,D}^{(k)}$ indicates that the D-dimensional filt-fPCs (or PCfPCs) representation is close to the D-dimensional ordinary fPC representation. The average values of $e_{v,D}^{(k)}$ across all tetrodes are displayed in Figure 10, which shows the overall better reconstruction performance of filt-fPCs.

The variance of the filt-fPC scores are displayed in Figures 4 and 5 in the Supplementary Material. A higher variation of common filt-fPCs indicates stronger functional connectivity of the associated brain subregions. In the postocclusion phase, tetrodes 11, 15, 16, and 17 are separated from the others in the first layer, and the shared common filt-fPCs explain a significant proportion of variation, which indicates that there could be nontrivial functional connectivity across these tetrodes, and the associated regions respond similarly to each other but distinctly from the other regions after the stroke onset. For tetrodes 6, 9, 10, 13, and

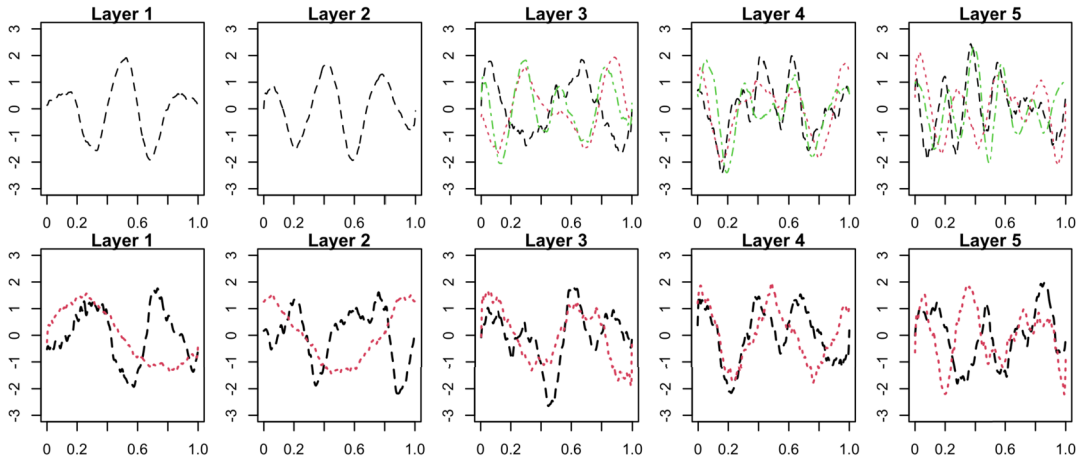

FIG. 9. *The directions of the estimated filt-fPCs of the first five layers. The upper five figures pertain to the preocclusion phase, and the lower five figures pertain to the postocclusion phase.*

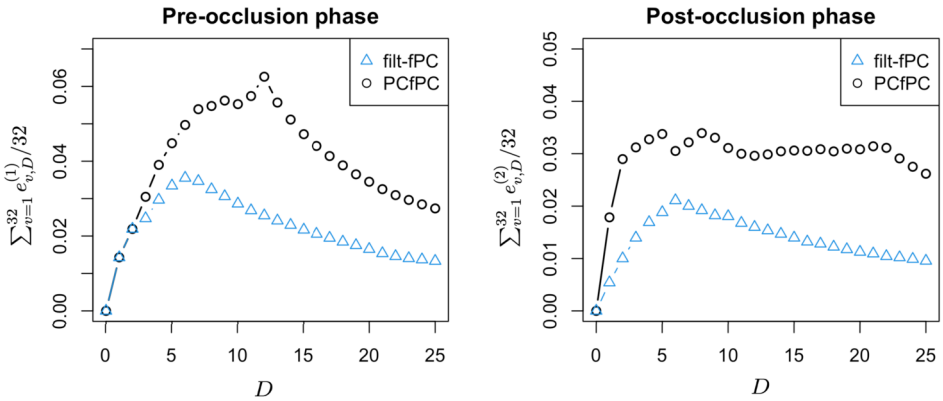

FIG. 10. *Average* $\{e_{v,D}^{(k)}: D = 1, \ldots, 25\}$ *across all tetrodes.*

27, the common filt-fPCs do not explain much data variation in both phases, indicating that these tetrodes are weakly interconnected with each other and the rest of the tetrodes. The tetrodewise values of $e_{v,D}^{(k)}$ are displayed in Figures 6 and 7 in the Supplementary Material. Clearly, for most tetrodes $e_{v,25}^{(k)} < 0.05$, and this means that the first 25 filt-fPCs can explain at least 95% variation explained by the groupwise ordinary fPCs. This justifies the efficiency of the selected filt-fPCs in functional reconstruction. For tetrodes 6, 9, 10, 13, 17, and 27, the PCfPC model leads to much worse reconstruction. In addition, for most $D = 1, \ldots, 25$, the $e_{v,D}^{(k)}$ value of PCfPC model is higher than that of filt-fPC model. That is because the variation pattern of epochs, collected from some tetrodes, for example, 6, 9, 10, 11, 13, 15, 16, 17, and 27, are substantially different from other tetrodes, and thus it is not advantageous to extract the common principal components for all the tetrodes jointly. In filt-fPCA these tetrodes are separated from the others in the first few layers, and thus the obtained filt-fPCs are more efficient. The results numerically justify the superiority of functional reconstruction of filt-fPCs.

6. Conclusions. Local field potentials provide information about brain function. The trajectories collected from different tetrodes simultaneously can be considered as multigroup functional data. Synchrony of different tetrodes potentially indicates functional connectivity of different regions of brain and a suddenly increased scale of spontaneous neuronal synchrony may antecede neuronal activity impairments in ischemic studies. The filt-fPCA is an efficient and effective method to extract and quantify the multilayer synchrony structure of multitetrode LFP recordings by employing filt-fPCs in a "multiresolution" way, and a data-driven algorithm is developed to find filt-fPCs. Specifically, we first specify a forest-structured community structure for the weighted network, established from data to measure the similarity of covariance structures of different tetrodes of LFP trajectories, and then find the common filt-fPCs for every community. The application of filt-fPCA to the local field potentials provides more sophisticated analysis on the synchrony. The method is developed *not* only for the LFP data described in this paper but also for all kinds of multigroup functional data, such as longitudinal functional data, multivariate functional data, and spatial-temporal data. Extending filtration techniques to functional linear models will be pursued as future work.

Acknowledgments. The authors would like to thank the anonymous referees, the Associate Editor, and the Editor for their constructive comments that substantially improved the quality of this paper.

SUPPLEMENTARY MATERIAL

Supplement to "Filtrated common functional principal component analysis of multigroup functional data" (DOI: 10.1214/23-AOAS1827SUPP; .pdf). The online Supplementary Material includes technical proofs, additional simulation and real data analysis results, and pseudocode for the developed community detection algorithm.

REFERENCES

BALI, J. L., BOENTE, G., TYLER, D. E. and WANG, J.-L. (2011). Robust functional principal components: A projection-pursuit approach. *Ann. Statist.* **39** 2852–2882. MR3012394 https://doi.org/10.1214/11-AOS923

BENKO, M., HÄRDLE, W. and KNEIP, A. (2009). Common functional principal components. *Ann. Statist.* **37** 1–34. MR2488343 https://doi.org/10.1214/07-AOS516

BERRENDERO, J. R., JUSTEL, A. and SVARC, M. (2011). Principal components for multivariate functional data. *Comput. Statist. Data Anal.* **55** 2619–2634. MR2802340 https://doi.org/10.1016/j.csda.2011.03.011

CHEN, K., DELICADO, P. and MÜLLER, H.-G. (2017). Modelling function-valued stochastic processes, with applications to fertility dynamics. *J. R. Stat. Soc. Ser. B. Stat. Methodol.* **79** 177–196. MR3597969 https://doi.org/10.1111/rssb.12160

CHEN, K. and MÜLLER, H.-G. (2012). Modeling repeated functional observations. *J. Amer. Statist. Assoc.* **107** 1599–1609. MR3036419 https://doi.org/10.1080/01621459.2012.734196

CHIOU, J.-M., CHEN, Y.-T. and YANG, Y.-F. (2014). Multivariate functional principal component analysis: A normalization approach. *Statist. Sinica* **24** 1571–1596. MR3308652

COFFEY, N., HARRISON, A. J., DONOGHUE, O. A. and HAYES, K. (2011). Common functional principal components analysis: A new approach to analyzing human movement data. *Hum. Mov. Sci.* **30** 1144–1166. https://doi.org/10.1016/j.humov.2010.11.005

CRAINICEANU, C. M., CAFFO, B. S., LUO, S., ZIPUNNIKOV, V. M. and PUNJABI, N. M. (2011). Population value decomposition, a framework for the analysis of image populations. *J. Amer. Statist. Assoc.* **106** 775–790. MR2894733 https://doi.org/10.1198/jasa.2011.ap10089

DI, C., CRAINICEANU, C. M. and JANK, W. S. (2014). Multilevel sparse functional principal component analysis. *Stat* **3** 126–143. MR4027332 https://doi.org/10.1002/sta4.50

DI, C.-Z., CRAINICEANU, C. M., CAFFO, B. S. and PUNJABI, N. M. (2009). Multilevel functional principal component analysis. *Ann. Appl. Stat.* **3** 458–488. MR2668715 https://doi.org/10.1214/08-AOAS206

FENG, Q., JIANG, M., HANNIG, J. and MARRON, J. S. (2018). Angle-based joint and individual variation explained. *J. Multivariate Anal.* **166** 241–265. MR3799646 https://doi.org/10.1016/j.jmva.2018.03.008

FLURY, B. K. (1987). Two generalizations of the common principal component model. *Biometrika* **74** 59–69. MR0885919 https://doi.org/10.1093/biomet/74.1.59

FLURY, B. N. (1984). Common principal components in k groups. *J. Amer. Statist. Assoc.* **79** 892–898. MR0770284

GREVEN, S., CRAINICEANU, C., CAFFO, B. and REICH, D. (2010). Longitudinal functional principal component analysis. *Electron. J. Stat.* **4** 1022–1054. MR2727452 https://doi.org/10.1214/10-EJS575

HALL, P. and HOSSEINI-NASAB, M. (2006). On properties of functional principal components analysis. *J. R. Stat. Soc. Ser. B. Stat. Methodol.* **68** 109–126. MR2212577 https://doi.org/10.1111/j.1467-9868.2005.00535.x

HALL, P., MÜLLER, H.-G. and WANG, J.-L. (2006). Properties of principal component methods for functional and longitudinal data analysis. *Ann. Statist.* **34** 1493–1517. MR2278365 https://doi.org/10.1214/009053606000000272

HAPP, C. and GREVEN, S. (2018). Multivariate functional principal component analysis for data observed on different (dimensional) domains. *J. Amer. Statist. Assoc.* **113** 649–659. MR3832216 https://doi.org/10.1080/01621459.2016.1273115

JACQUES, J. and PREDA, C. (2014). Model-based clustering for multivariate functional data. *Comput. Statist. Data Anal.* **71** 92–106. MR3131956 https://doi.org/10.1016/j.csda.2012.12.004

JIANG, C.-R. and WANG, J.-L. (2010). Covariate adjusted functional principal components analysis for longitudinal data. *Ann. Statist.* **38** 1194–1226. MR2604710 https://doi.org/10.1214/09-AOS742

JIAO, S., FROSTIG, R. D. and OMBAO, H. (2023). Break point detection for functional covariance. *Scand. J. Stat.* **50** 477–512. MR4599922 https://doi.org/10.1111/sjos.12589

JIAO, S., FROSTIG, R. and OMBAO, H. (2024). Supplement to "Filtrated common functional principal component analysis of multigroup functional data." https://doi.org/10.1214/23-AOAS1827SUPP

KAYANO, M. and KONISHI, S. (2009). Functional principal component analysis via regularized Gaussian basis expansions and its application to unbalanced data. *J. Statist. Plann. Inference* **139** 2388–2398. MR2508000 https://doi.org/10.1016/j.jspi.2008.11.002

LOCK, E. F., HOADLEY, K. A., MARRON, J. S. and NOBEL, A. B. (2013). Joint and individual variation explained (JIVE) for integrated analysis of multiple data types. *Ann. Appl. Stat.* **7** 523–542. MR3086429 https://doi.org/10.1214/12-AOAS597

NISHII, R. (1984). Asymptotic properties of criteria for selection of variables in multiple regression. *Ann. Statist.* **12** 758–765. MR0740928 https://doi.org/10.1214/aos/1176346522

RAMSAY, J. O. and SILVERMAN, B. W. (2005). *Functional Data Analysis*, 2nd ed. *Springer Series in Statistics*. Springer, New York. MR2168993

SCHOTT, J. R. (1999). Partial common principal component subspaces. *Biometrika* **86** 899–908. MR1741985 https://doi.org/10.1093/biomet/86.4.899

WANG, B., LUO, X., ZHAO, Y. and CAFFO, B. (2021). Semiparametric partial common principal component analysis for covariance matrices. *Biometrics* **77** 1175–1186. MR4357829 https://doi.org/10.1111/biom.13369

WANN, E. G. (2017). Large-scale spatiotemporal neuronal activity dynamics predict cortical viability in a rodent model of ischemic stroke. Ph.D. thesis, UC Irvine.

YAO, F. (2007). Functional principal component analysis for longitudinal and survival data. *Statist. Sinica* **17** 965–983. MR2408647

YAO, F. and LEE, T. C. M. (2006). Penalized spline models for functional principal component analysis. *J. R. Stat. Soc. Ser. B. Stat. Methodol.* **68** 3–25. MR2212572 https://doi.org/10.1111/j.1467-9868.2005.00530.x

ZHANG, Y., LI, R. and TSAI, C.-L. (2010). Regularization parameter selections via generalized information criterion. *J. Amer. Statist. Assoc.* **105** 312–323. With supplementary material available online. MR2656055 https://doi.org/10.1198/jasa.2009.tm08013